Geophysical Research Letters

RESEARCH LETTER
10.1029/2023GL105183

Effects of Mixing at Pore Intersections on Large-Scale Dissolution Patterns and Solute Transport

Rishabh P. Sharma[1], Jingxuan Deng[2,3], Peter K. Kang[2,3], and Piotr Szymczak[1]

[1]Institute of Theoretical Physics, Faculty of Physics, University of Warsaw, Warsaw, Poland, [2]Department of Earth and Environmental Sciences, University of Minnesota, Minneapolis, MN, USA, [3]Saint Anthony Falls Laboratory, University of Minnesota, Minneapolis, MN, USA

Key Points:

- Mixing at pore intersections can have a major impact on macroscopic dissolution patterns and solute transport
- Mixing effect is the strongest when reactive and advective time scales in the system are comparable
- Mixing effect on dissolution increases as network heterogeneity decreases

Correspondence to:

P. Szymczak and P. K. Kang,
piotrek@fuw.edu.pl;
pkkang@umn.edu

Citation:

Sharma, R. P., Deng, J., Kang, P. K., & Szymczak, P. (2023). Effects of mixing at pore intersections on large-scale dissolution patterns and solute transport. *Geophysical Research Letters*, *50*, e2023GL105183. https://doi.org/10.1029/2023GL105183

Received 26 JUN 2023
Accepted 30 SEP 2023

Author Contributions:

Conceptualization: Peter K. Kang, Piotr Szymczak
Data curation: Rishabh P. Sharma, Jingxuan Deng
Formal analysis: Rishabh P. Sharma, Jingxuan Deng
Funding acquisition: Peter K. Kang, Piotr Szymczak
Investigation: Rishabh P. Sharma, Jingxuan Deng, Peter K. Kang, Piotr Szymczak
Methodology: Rishabh P. Sharma, Jingxuan Deng, Peter K. Kang, Piotr Szymczak
Project Administration: Peter K. Kang, Piotr Szymczak
Resources: Peter K. Kang, Piotr Szymczak
Software: Rishabh P. Sharma, Jingxuan Deng

Abstract The flow-induced dissolution of porous rocks governs many important subsurface processes and applications. Solute mixing, which determines pore-scale concentration fields, is a key process that affects dissolution. Despite its importance, the effects of pore-scale mixing on large-scale dissolution patterns have not been investigated. Here, we use a pore network model to elucidate the mixing effects on macroscopic dissolution patterns and solute transport. We consider two mixing rules at pore intersections that represent two end members in terms of the mixing intensity. We observe that the mixing effect on dissolution is the strongest at moderate Damköhler number, when the reactive and advective time scales are comparable. This is the regime where wormholes spontaneously appear. Incomplete mixing is shown to enhance flow focusing at the tips of the dissolution channels, which results in thinner wormholes and shorter breakthrough times. These effects on passive solute transport are evident independent of initial network heterogeneity.

Plain Language Summary When a reactive fluid infiltrates the rock, the dissolution channels (wormholes) can spontaneously form, in which the flow and transport of reactant focus. The formation and growth of such channels is a complex phenomenon in which the processes taking place at the micro-scale are strongly coupled with the macro-scale patterns. One of these processes is the mixing of reactant-saturated water at pore intersections. In this paper, we study how the intensity of the mixing process impacts the shapes and growth velocities of the dissolution channels. We find that when the mixing at pore intersections is relatively weak, the flow focuses more strongly in front of the wormhole tip, which reduces the width of the wormhole and leads to its faster propagation and early breakthrough. These effects are also evident from tracer breakthrough curves. Our findings contribute to the understanding of dissolution-induced patterns, with implications to subsurface flow-related processes such as karst formation and contaminant migration.

1. Introduction

The dissolution of porous and fractured media is a complex process where the nonlinear coupling of flow, transport, reaction, and pore geometry evolution leads to the formation of a variety of shapes and patterns (Jamtveit & Hammer, 2012; Steefel & Maher, 2009). Depending on the flow conditions and pore space geometry, three different dissolution regimes emerge (Fredd & Fogler, 1998; Golfier et al., 2002; Ladd & Szymczak, 2021). If the reactant penetration length is much shorter than the system length, the dissolution is limited to the surface of the rock (face dissolution regime). In the other extreme, at high flow rates, when the penetration length is much longer than the system length, the sample dissolves uniformly, without any significant porosity gradients developing along the flow direction. Finally, for intermediate flow rates, the flow self-organizes in the dissolution channels (wormholes), which form a fractal network throughout the sample (Chadam et al., 1986; Daccord, 1987; Hoefner & Fogler, 1988; Menke et al., 2017; Szymczak & Ladd, 2009).

The flow-focusing instability has been known for a long time in the petroleum industry (Rowan, 1959), where it was used to increase the effectiveness of carbonate reservoir stimulation techniques. In that context, it has also been studied experimentally (Fredd & Fogler, 1998; Hoefner & Fogler, 1988) and numerically (Cohen et al., 2008; Maheshwari & Balakotaiah, 2013; Panga et al., 2005). In the physics community, the interest in these systems has been sparked by classical papers of Daccord and Lenormand, which analyzed the patterns formed in a dissolving plaster and related them to other pattern-forming systems, such as diffusion-limited aggregation (Daccord, 1987; Daccord & Lenormand, 1987). Recent years have seen a growing number of experimental studies of dissolution-induced morphology evolution (Luquot et al., 2014; Noiriel et al., 2013; Polak et al., 2004),

Supervision: Peter K. Kang, Piotr Szymczak
Validation: Rishabh P. Sharma, Piotr Szymczak
Visualization: Rishabh P. Sharma, Jingxuan Deng, Peter K. Kang
Writing – original draft: Rishabh P. Sharma, Peter K. Kang, Piotr Szymczak
Writing – review & editing: Peter K. Kang, Piotr Szymczak

many of them in the context of CO_2 sequestration (Carroll et al., 2013; Deng et al., 2013; J. Elkhoury et al., 2015; J. E. Elkhoury et al., 2013; Ellis et al., 2011; Hao et al., 2013; Luquot & Gouze, 2009). Since many of the potential reservoirs for CO_2 storage are in carbonate strata, it is crucial to understand how the flow of CO_2-acidified brine impacts the long-term changes in porosity and permeability of the reservoirs and how it affects the caprock properties.

In karst studies, the understanding of the profound role that flow-focusing plays in the pattern development came with the pioneering work of Ewers (1982), who analyzed a number of analog models of karst formation, made of plaster of Paris. This study has provided a number of important insights into the process of cave formation, and the role of flow focusing in this process. Further insight into flow-focusing effects has been provided by numerical modeling of the early stages of karst development (Chaudhuri et al., 2013; Cheung & Rajaram, 2002; Groves & Howard, 1994; Hanna & Rajaram, 1998; Szymczak & Ladd, 2011; Worthington & Ford, 2009).

Macroscopic rock dissolution pattern is the result of pore-scale reactive transport. The complex interplay between reactant transport via advection and diffusion in the pore bodies and chemical reaction at the rock surfaces governs the dissolution at the pore scale. However, the magnitude of the flow and the concentration profile in the sample are global in nature, and sensitive to the presence of preferential flow paths or large-scale inhomogeneities. These micro- to macro-scale couplings may be significantly enhanced by the dissolution, particularly in the unstable regime, where existing flow paths are amplified and new ones appear (Menke et al., 2016; Upadhyay et al., 2015).

Understanding the effects of pore-scale phenomena on larger-scale processes has been of great interest for upscaling subsurface processes (Battiato & Tartakovsky, 2011; Hu et al., 2021; Kang et al., 2019). Recent studies indeed showed that macroscopic reactive transport can be governed by pore-scale properties such as pore network structure and pore-scale mineral distribution (Li et al., 2007; Roded et al., 2021). Also, pore-scale transport processes such as mixing are shown to greatly affect effective surface reaction rates (Deng et al., 2018; W. Lee et al., 2023; Li et al., 2006; Liu et al., 2022).

Mixing is a key pore-scale process in reactive flows because it controls the transport of reactive solutes to and from the surfaces of the pores, and mixing-induced reactions (Dentz et al., 2011). In particular, mixing at pore junctions and fracture intersections has been of research interest because the intersections are where fluids with different properties can vigorously mix and react (Berkowitz et al., 1994; Stockman et al., 2001; Zou et al., 2017). For example, recent studies highlighted that fracture intersections can be potential biogeochemical reaction hot spots (Bochet et al., 2020; S. H. Lee & Kang, 2020). Further, previous studies have shown that the mixing extent at pore intersections can govern larger-scale solute spreading (Kang et al., 2015; Park et al., 2001; Sherman et al., 2019). This implies that the dissolution patterns could also be governed by mixing at intersections, and recent studies showed that a wide range of mixing conditions can occur at intersections (S. H. Lee & Kang, 2020; Zou et al., 2017). However, most network-scale dissolution models (if not all) have been assuming well-mixed conditions at intersections. This is mainly because currently there is no universal, coarse-grained mixing rule that quantifies the amount of mixing at intersections. Pore-scale simulations have to be conducted to accurately estimate the mixing extent at intersections because the mixing at intersections depends not only on local Péclet number but also on detailed intersection geometry and incoming fluxes (Zou et al., 2017). Thus, the effects of solute mixing at pore intersections on large-scale dissolution patterns have been unclear.

Here, we study the effects of the mixing of reactive solutes at pore junctions on large-scale dissolution patterns and solute transport. For this purpose, we implemented two mixing rules at pore junctions into the pore network model of a dissolving porous medium. Full mixing assumes that the solute transport at pore junctions is diffusion-dominated such that reactive solutes become well mixed. On the other hand, streamline routing assumes that the system is advection-dominated such that reactive solutes follow streamlines and do not transition between streamlines at pore junctions. This leads to partial mixing or no mixing of incoming concentration at junctions. We found that the interplay between network conductivity heterogeneity and mixing strongly affects the macroscopic dissolution patterns and resulting tracer (passive solute) transport, and we elucidated the underlying mechanisms.

2. Pore Network Model

To investigate the coupling between the pore-scale mixing processes and macroscopic dissolution patterns, we use the capillary pore network model of a dissolving porous medium. Network models introduce a simplified representation of a porous material, either as a network of interconnected capillaries (Budek & Szymczak, 2012;

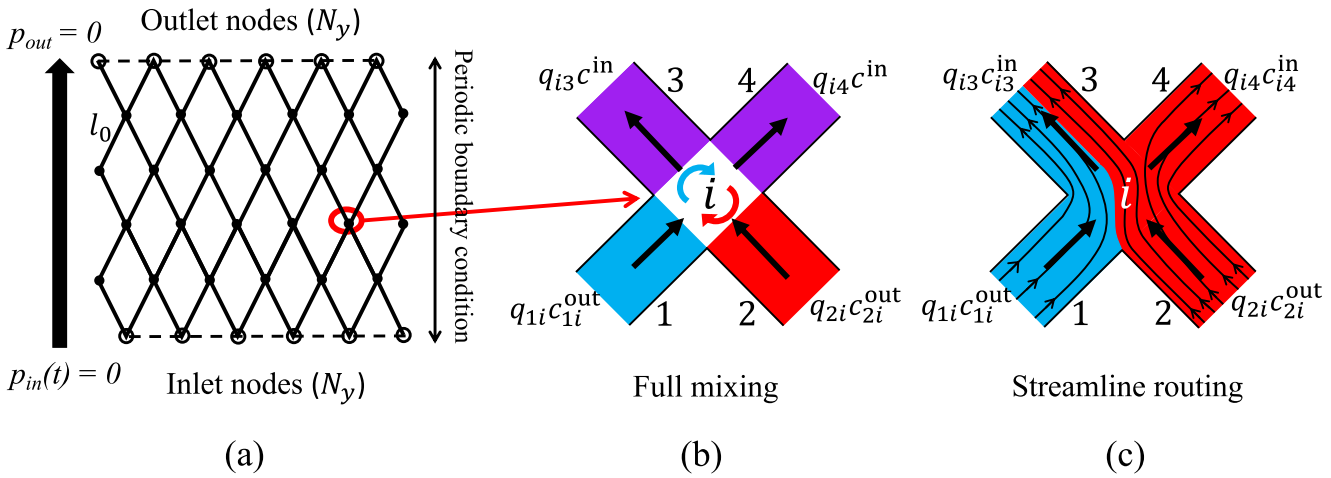

Figure 1. (a) A schematic representation of a network with rhombic lattice and linear inlet and outlet. (b) Full mixing: Junction i is fed by two solute fluxes with concentrations c_{1i}^{out} and c_{2i}^{out} from pore outlets 1 and 2 respectively. After full mixing, a final concentration c^{in} flows into pores 3 and 4. The color indicates different concentrations. (c) Streamline routing: Concentration fluxes follow the streamlines. The concentrations entering pores 3 and 4 from node i are $c_{i3}^{in}$and c_{i4}^{in} respectively.

Hoefner & Fogler, 1988; Roded et al., 2020, 2021) or as spherical pore bodies connected by cylindrical throats (Blunt et al., 2013; De Boever et al., 2012; Nogues et al., 2013; Raoof et al., 2012; Tansey & Balhoff, 2016; Xiong et al., 2016), offering a compromise between the computational accuracy characterizing the pore-scale models and the ability to tackle large-scale problems, which are the advantages of Darcy-scale methods. Pore-network models allow for control of the pore architecture (diameters, lengths, connectivity), tuning it to represent different rocks. In dissolution problems, pore network models are able to correctly reproduce the competition between the individual pores for the reactant flux, which leads to a successful representation of the variety of spontaneously formed dissolution patterns such as wormholes (Ameri et al., 2017; Budek & Szymczak, 2012), including their structure and advancement rate, permeability evolution, and the non-monotonic relationship between injection rate and fluid volume required for breakthrough (Budek & Szymczak, 2012; Fredd & Fogler, 1998; Hoefner & Fogler, 1988). They were also successfully used to analyze the link between pore-scale features and large-scale morphologies (Roded et al., 2020, 2021).

In this study, we represent a porous rock as a network of cylindrical capillaries (of initially heterogeneous sizes) that are broadened by the dissolution (Budek & Szymczak, 2012; Hoefner & Fogler, 1988; Roded et al., 2021). The nodes of the network (pore junctions) are assumed to be volumeless such that all the reaction takes place in the capillaries (pores) only. The nodes are placed on a regular lattice with the link length of constant l_0, as shown in Figure 1. Such geometry with four branch intersections is particularly well suited to study the mixing effects (Hull & Koslow, 1986; Kang et al., 2011, 2017). In the limiting case of short residence times at the intersection and uniform pore diameters, the two incoming tracer streams will remain unmixed in this geometry. Heterogeneity in the network is introduced by assigning an initial diameter to each tube according to log-normal distribution with mean d_0 and standard deviation σ. The log-normal distribution is used here based on its ubiquity in many natural systems (Sanchez-Vila et al., 2006), and a wide range of σ is considered to study the effects of initial network heterogeneity.

The reactive fluid is injected into the system through the set of N_y inlet nodes (Figure 1) where the pressure $p_{in}(t)$ is imposed, and leaves the system through outlet nodes where the pressure is kept at zero, $p_{out}(t) = 0$. The inlet pressure is adjusted in each time step to keep the total volumetric flow rate through the system, Q_0, constant. The fluid is assumed to be incompressible and the flow in each pore is considered to be laminar and fully developed. For a pore (ij) joining nodes i and j, the flow rate (q_{ij}) is then given by the Hagen–Poiseuille equation

$$q_{ij} = -\frac{\pi d_{ij}^4}{128\mu l_0}(p_i - p_j) \quad (1)$$

where d_{ij} is the diameter of the pore ij and l_0 is the length of a pore, uniform throughout the network. Next, μ is the dynamic viscosity of the fluid, and p_i is the pressure at node i. The hydraulic conductance of a capillary tube

that relates volumetric flux (q) and pressure drop can be defined as $\frac{\pi d_{ij}^4}{128\mu l_0}$, and the initial network heterogeneity is quantified by computing the log-variance of hydraulic conductance, σ^2. At each node, we also have a continuity condition

$$\sum_j q_{ij} = 0 \tag{2}$$

where the sum is over all the nodes connected by a pore with node j. The resulting system of sparse linear equations can then be solved for pressure values at the nodes.

We now introduce reactant into this system through the inlet face, by imposing the constant concentration condition $c = c_{\text{in}}$ there. The reactant is consumed in the pores, with the rate which is assumed to be linear in c

$$R = \frac{k}{1 + \frac{kd_{ij}}{D\text{Sh}}} c \equiv k_{\text{eff}}(d_{ij})c \tag{3}$$

here k is the surface reaction rate, D is the diffusion coefficient of the reactant and d_{ij} is the diameter of the pore connecting nodes i and j. Finally, Sh is the Sherwood number, which is the non-dimensional mass transfer coefficient (Bejan, 1984; Gupta & Balakotaiah, 2001), characterizing the intensity of the diffusive current to the reactive wall. The parameter $g = \frac{kd_{ij}}{D\text{Sh}}$ in the denominator of Equation 3 accounts for the hindering effect of diffusion on the dissolution rate, particularly pronounced in wider pores. As a result, the pore surfaces tend to react with a slower effective rate, k_{eff}, which includes the transverse diffusion effect. For narrow pores or low reaction rates ($g \ll 1$) dissolution is reaction-limited ($k_{\text{eff}} \approx k$) and diffusion is fast enough to maintain the uniform concentration profile along the diameter of the pore. When the pores are large or reaction rates are high then dissolution becomes transport limited ($g \gg 1$), and the effective reaction rate is controlled by diffusion. The Sherwood number itself depends on kd/D, but the variation is relatively small (Gupta & Balakotaiah, 2001), bounded by two asymptotic limits; high reaction rates (transport limit) and low reaction rates (reaction limit). For our geometry (circular) these limits correspond to Sh = 4.861 and Sh = 5.385, respectively (Ebadian & Dong, 1998). In this study, we approximate Sh by a constant value Sh = 5.

The reaction at the pore surface will lead to the decay of the concentration along the pore according to

$$q_{ij}\frac{dc}{dx} = -\pi d_{ij} k_{\text{eff}} c \tag{4}$$

where q_{ij} is the volumetric flow rate in pore ij and the diffusion along the axial coordinate (x) was neglected. Equation 4 can be solved analytically in a pore with a uniform diameter yielding

$$c(x) = c_{ij}^{\text{in}} e^{-\frac{\pi d_{ij} k_{\text{eff}}}{q_{ij}} x} \tag{5}$$

where c_{ij}^{in} is the concentration at the inlet of pore ij. In particular, the concentration at the end of the pore ij will be equal to

$$c_{ij}^{\text{out}} = c_{ij}^{\text{in}} e^{-\frac{\pi d_{ij} k_{\text{eff}}}{q_{ij}} l_0} \tag{6}$$

The equations analogous to (5) can be written for each pore in the sample. However, in order to calculate the concentration values at all of the nodes in the network, these relations need to be supplemented with the mixing rules at the intersections. Traditionally, a full mixing assumption is adopted, which assumes that the concentration in the node is just the flow-weighted average of incoming concentrations. To be more precise, for a node i, with incoming concentrations c_{ji}^{out} from pore outlets (j), the final outgoing concentration c_{ik}^{in} to the pore inlets (k) is:

$$c_{ik}^{\text{in}} = \left(\sum_j q_{ji} c_{ji}^{\text{out}}\right) \Big/ \left(\sum_j q_{ji}\right) \tag{7}$$

where the sum is taken over the pores (ji) connected to node i which are bringing the flow in and ik is one of the outgoing pores. Equations 6 and 7 form again a sparse linear system, which can be solved for the concentration values at the nodes.

The final element of the model is the erosion equation, which governs the evolution of the pore diameters

$$\partial_t(d_{ij}/2) = \frac{k_{\text{eff}}}{\nu c_{\text{sol}}} c. \tag{8}$$

where c_{sol} is the molar concentration of soluble material and ν accounts for the stoichiometry of the reaction. The total volume of a mineral dissolved from the walls of a pore of diameter d over time Δt is then

$$\Delta V = \frac{\pi d k_{\text{eff}} \Delta t}{\nu c_{\text{sol}}} \int_0^l c(z) dz = \Delta t q \frac{c_0}{c_{\text{sol}} \nu} \left(1 - e^{-\pi d k_{\text{eff}} l/q}\right). \tag{9}$$

In order to keep the model tractable, we assume that the pores are broadening uniformly along their length (Fredd & Fogler, 1998; Hoefner & Fogler, 1988). Thus, the above volume change corresponds to the enlargement of the pore diameter by

$$\Delta d = \frac{\Delta V}{\pi d l} = \frac{2\Delta t q}{\pi d l} \frac{c_0}{c_{\text{sol}} \nu} \left(1 - e^{-\pi d k_{\text{eff}} l/q}\right). \tag{10}$$

The details of the implementation together with explicit formulas for the pore growth can be found in Budek and Szymczak (2012).

2.1. Dimensionless Numbers

As mentioned above, the ratio $g = \frac{k d_{ij}}{D\text{Sh}}$ describes the relative magnitude of reaction and transverse diffusion across the pore. The characteristic value of this parameter

$$G = \frac{k d_0}{D\text{Sh}} \tag{11}$$

is thus a dimensionless number characterizing the hindering effect of the diffusive transport on the dissolution rate throughout the sample.

Another important parameter is an effective Damköhler number, which is defined by the combination of parameters in the exponent of Equation 6

$$\text{Da}_{\text{eff}} = \frac{\pi d_0 k_{\text{eff}} l_0}{q_0} = \frac{\pi d_0 k l_0}{q_0 (1 + G)} \tag{12}$$

where q_0 is a characteristic initial volumetric flux in a pore, $q_0 = Q_0/2N_y$. Note that Péclet number can be expressed through Da_{eff} and G, and Da_{eff} has been shown to exert a strong control over dissolution patterns compared to G (Budek & Szymczak, 2012).

The effective Damköhler number characterizes the penetration length of the reactant in the sample

$$l_p = \frac{l_0}{\text{Da}_{\text{eff}}} \tag{13}$$

Finally, we define the dimensionless time $\hat{t}$ which is given by

$$\hat{t} = \frac{2k\gamma t}{d_0}, \tag{14}$$

where $\gamma = c_0/\nu c_{\text{sol}}$ is the acid capacity number which is defined as the number of molecules per unit volume of a mineral to the number of molecules of reactant per unit volume of incoming fully saturated fluid.

2.2. Incomplete Mixing

Full mixing at the intersections, as described by Equation 7 can be physically realized if the residence times of the solute at the intersections are sufficiently large. For shorter residence times (corresponding to higher flow rates), the mixing is incomplete, with a considerable portion of reactant following the streamlines. In the limit of zero residence this results in *streamline routing*. Equation 7 is then replaced by:

$$c_{ik}^{\text{in}} = \left(\sum_j \alpha_{jk} q_{ji} c_{ji}^{\text{out}}\right) \Big/ \left(\sum_j \alpha_{jk} q_{ji}\right) \tag{15}$$

where α_{jk} is the fraction of flow from the pore ji that makes it to the pore ik. Note that if α_{jk} is a constant (independent of j and k) then streamline routing reduces to the full mixing rules. Figures 1b and 1c illustrate the full mixing and streamline routing in the diamond lattice where the incoming concentration c_{1i}^{out} from pore 1 is shown in blue and c_{2i}^{out} from pore 2 is marked in red. Pore 2 is assumed to have a higher volumetric flow rate than pore 4, ($q_{2i} > q_{i4}$). In the case of complete mixing, the resulting outgoing concentration (c^{in}) is forwarded to pores 3 and 4 (violet). In the streamline routing case (Figure 1b) pore 3 will get both the reactant flux from pore 1 as well as part of the flux from pore 2 while the remaining flux is forwarded to pore 4. The reactant transfer probabilities are then $\alpha_{13} = 1$, $\alpha_{14} = 0$, $\alpha_{23} = (q_{2i} - q_{i4})/q_{2i}$, and $\alpha_{24} = q_{i4}/q_{2i}$. The outgoing concentrations are then given by

$$c_{i3}^{\text{in}} = \frac{q_{1i}c_{1i}^{\text{out}} + (q_{2i} - q_{i4})c_{2i}^{\text{out}}}{q_{i3}} \tag{16}$$

$$c_{i4}^{\text{in}} = c_{2i}^{\text{out}} \tag{17}$$

The transfer probabilities for $q_{i4} > q_{2i}$ (or, equivalently, $q_{i3} < q_{1i}$) can be obtained by an appropriate permutation of indices in the above expression (Kang et al., 2015; Park et al., 2001). Finally, in the case when there is just one inlet pore distributing the fluid to three outlet pores or three inlet pores with one outlet, the streamline routing gives identical results to full mixing, thus Equation 7 can then be used.

The choice of mixing protocol in a given physical situation depends on the local Péclet number characterizing the flow through the intersection, Pe_{int}. This number is equal to the ratio of the advective travel time through the intersection, d_{int}/v, to the respective diffusive time, d_{int}^2/D, with d_{int}—a characteristic size of an intersection. The intersection Péclet number is then $\text{Pe}_{\text{int}} = d_{\text{int}}v/D$, with $\text{Pe}_{\text{int}} > 1$ leading to streamline routing, and $\text{Pe}_{\text{int}} \ll 1$ defining the range over which full mixing assumption should work well. In natural and laboratory systems, one encounters a large range of Pe_{int}. Taking as an example the acidization of Indiana limestone (Hoefner & Fogler, 1988), where v is in the range $0.05 - 5$ cm/s, $D = 3.6 \times 10^{-5}$ cm^2/s (Fredd & Fogler, 1998) and $d_{\text{int}} \approx 5$ μm (Freire-Gormaly et al., 2016), we get Pe_{int} in the range $0.5 - 50$, depending on the flow rate used. On the other hand, groundwater flows in natural rocks are much lower, usually in the range 10^{-8}–10^{-5} cm s^{-1} (Lake et al., 2002), which leads to $\text{Pe}_{\text{int}} \ll 1$. A substantially different situation is encountered for the dissolution of rock fractures or bedding planes. Such systems can be simulated using the present model, with the 2D network of channels then representing the flow paths in the fracture plane, around the asperities. Fracture apertures are between 0.005 and 0.1 cm (Dreybrodt, 1996; Motyka & Wilk, 1984; Paillet et al., 1987), and hydraulic gradients are of the order of 10^{-3} to 10^{-1} (Dijk & Berkowitz, 1998; Palmer, 1991). This gives a range of characteristic flow velocities in undissolved fractures from 10^{-4} to 1 cm/s. The corresponding intersection Péclet numbers are then $0.05 < \text{Pe}_{\text{int}} < 10^4$, taking the fracture aperture as the characteristic intersection size and assuming the solute diffusion coefficient of $D = 10^{-5}$ cm^2 s^{-1}. The above shows that a wide range of Péclet numbers can be encountered when dissolving fractured and porous rocks, which implies that both mixing rules can commonly occur in nature.

3. Results and Discussion

To investigate the effects of mixing at the pore intersections on the macro-scale dissolution patterns, we have carried out a large number of dissolution simulations on the 200×200 lattice implementing both the full mixing rule (7) as well as the streamline routing protocol (15). The simulations were performed over a large range of effective Damköhler number, $0.01 < \text{Da}_{\text{eff}} < 1.0$. Outside of this range, the dissolution is either uniform (small Da_{eff}) due to a large penetration length or results in face dissolution due to a very short penetration length (large Da_{eff}) (Budek & Szymczak, 2012). The simulations were performed with a fixed value of G parameter, G = 1, which implies a mixed transport/reaction control on the dissolution rate, characteristic of acidization experiments. For example, dissolution of Indiana limestone by hydrochloric acid with surface reaction rate $k = 0.2$ cm/s results in $\text{G} \approx 0.7$. The impact of G on the pattern is known to be much weaker than that of Da_{eff} (Budek & Szymczak, 2012), mostly affecting the diameters of the dissolving pores around the inlet, which decrease with increasing G. A wide range of σ^2 (log-variance of initial conductance distribution) is also considered to investigate the effects of initial network heterogeneity.

Figure 2 shows the simulated dissolution patterns for different Da_{eff} and initial pore heterogeneities characterized by σ^2. Simulations were stopped when at least one pore along the line $x = L_x/2$ increases its diameter by a factor of five, which we define as half breakthrough time. Note that L_x is the domain size in the flow direction, x.

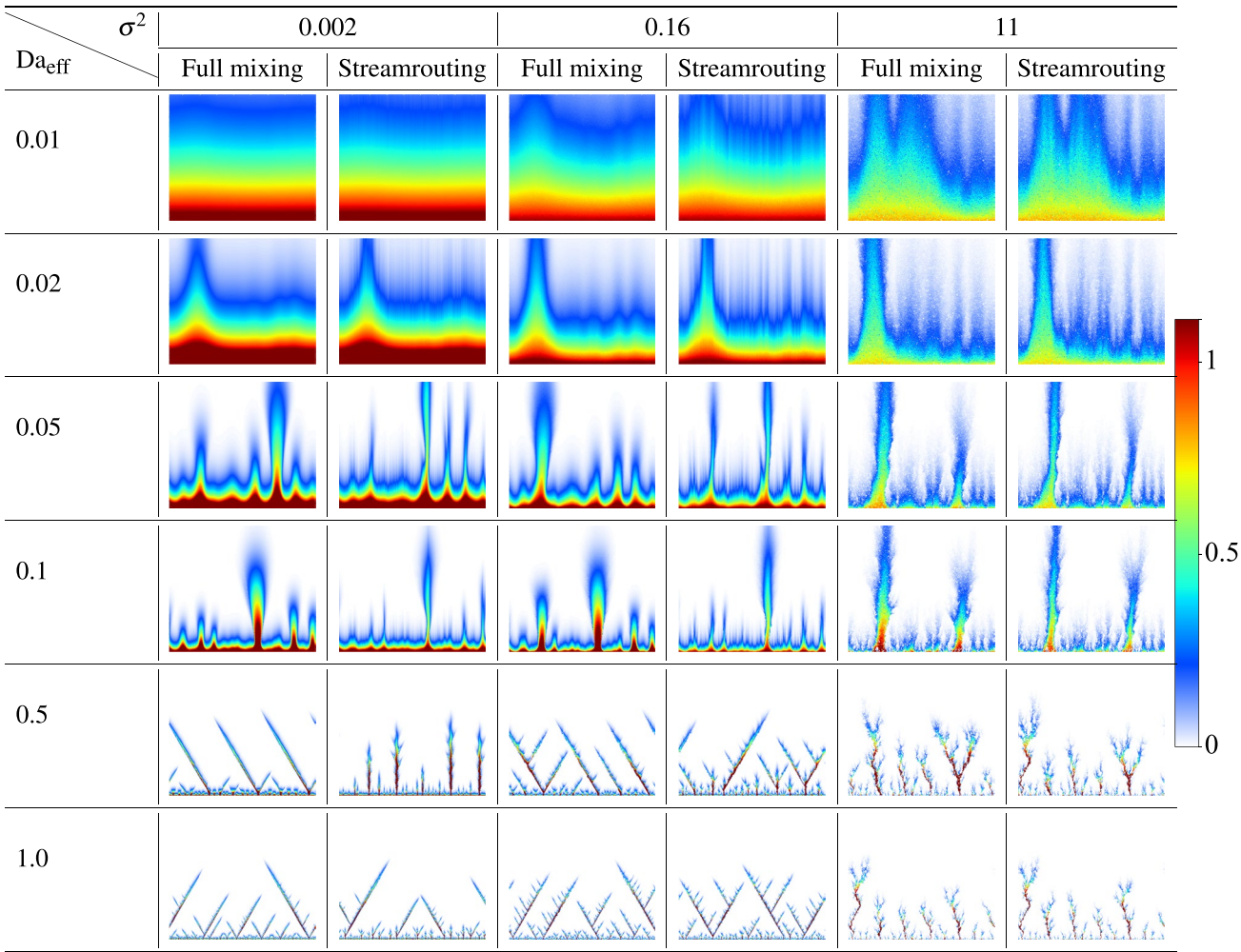

Figure 2. Dissolution patterns for different mixing rules as a function of effective Damköhler number (Da_{eff}) and initial heterogeneity of the network. Initial pore diameters are distributed log-normally, and σ^2 is the log-variance of initial hydraulic conductance values. The colors represent the growth of pore diameters ($d_{ij}(t) - d_{ij}(0)$). To better visualize the dissolution patterns, we increased the widths of the lines with which we plot individual pores to three times the diameter of each pore ($3d_{ij}$). The successive shadings indicate large chemical erosion (dark red), intermediate erosion (yellow and green), low erosion (blue), and no erosion (white).

We observe that in the uniform dissolution regime with a small effective Damköhler number ($Da_{eff} \leq 0.02$) both types of mixing produce similarly shaped patterns as the reactant invades the whole network due to a large penetration length (l_p). Coming back to Figures 1b and 1c, note that if both incoming pores at a given intersection have the same incoming concentration $\left(c_{1i}^{out} \approx c_{2i}^{out}\right)$ then the outgoing concentrations are also the same $\left(c_{i3}^{in} = c_{i4}^{in} = c_{1i}^{out}\right)$, independently of the mixing mechanism. This results in an even distribution of reactant throughout the pores, irrespective of their hydraulic resistance. However, as Da_{eff} increases, the penetration length l_p becomes shorter, and dissolution becomes more localized. The reactant is consumed faster locally by competing flow paths which results in the faster growth of the winning ones which further focuses more flow in just a handful of dissolution channels. In this Da_{eff} regime ($0.05 < Da_{eff} < 0.1$), streamline routing produces thinner channels in comparison to full mixing.

To understand this effect, let us first comment on the impact of mixing protocol on the value of transverse dispersion in the network. For a homogeneous diamond network, the streamline routing transfer probabilities α_{jk} at the intersection (Figure 1c) reduce to $\alpha_{13} = 1$, $\alpha_{14} = 0$, $\alpha_{23} = 0$ and $\alpha_{24} = 1$. This results in the transfer of concentrations in a mean flow direction (from pore 1 to pore 3 and from pore 2 to pore 4) without any transverse dispersion. On the contrary, in the case of full mixing, the concentration is distributed uniformly in the outgoing pores with $\alpha_{jk} = 1/2$ regardless of the flow. This gives rise to the appearance of a Saffman-type dispersion (Saffman, 1959), with the tracer spreading in the transverse direction. For a fully homogeneous system, the transverse dispersion

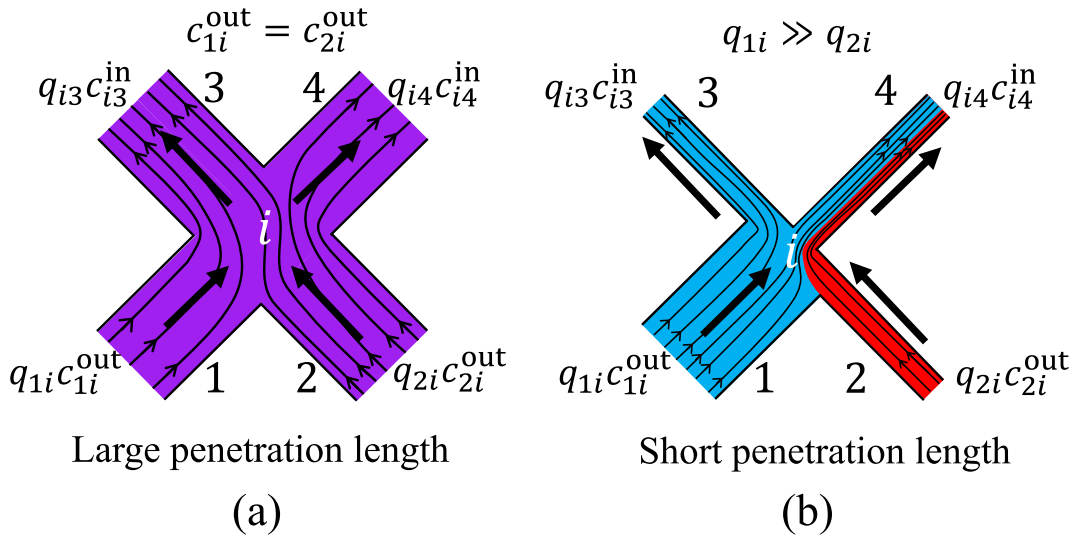

Figure 3. Two different scenarios in which streamline routing behaves similarly to full mixing (a) Large penetration length (l_p) where concentrations (violet color) from both pore outlets 1 and 2 are the same ($c_{1i}^{out} = c_{2i}^{out}$) and the resulting final concentration $\left(c_{i3}^{in} = c_{i4}^{in} = c_{2i}^{out}\right)$ enters in pore 3 and 4 (b) Small penetration length with pore 1 having larger flow rate ($q_{1i} \gg q_{2i}$). The respective concentration c_{1i}^{out} (blue color) dominates the junction and is forwarded to both pores 3 and 4.

coefficient for full mixing can be calculated to be $D_T^{fm} = 1/4ul_0$, where u is the average flow rate in the pore. A similar calculation for streamline routing yields $D_T^{sr} = 0$, which reflects the fact that the concentration is simply transmitted from pore to pore, without spreading. Naturally, for a heterogeneous network D_T^{sr} will have a finite value, but the magnitude of D_T^{sr} is still expected to be considerably smaller than the corresponding value of D_T^{fm}. The next observation is that, as argued in Steefel and Lasaga (1990) the width of the dissolution channel is proportional to $\sqrt{D_T}$, hence the channels should be wider in the case of full mixing, which is indeed observed. However, as system heterogeneity increases, many of the transfer coefficients α_{jk} become nonzero, and there is an appreciable redistribution of the reactant between the outgoing pores for both mixing protocols (Kang et al., 2015). Thus, we expect that the differences in channel width produced by different mixing rules decrease with increasing heterogeneity.

At moderate and large Damköhler numbers, $Da_{eff} \geq 0.5$, the penetration length l_p becomes comparable with the pore length, and the strong competition for the reactant appears at the level of individual pores. The pores getting larger flow consume more reactant and grow at a faster rate. In heterogeneous systems (e.g., $\sigma^2 = 11$), this results in the formation of highly branched fractal-shaped dissolution patterns with a width comparable to that of a single pore. In this regime of system growth, the effect of mixing rules is rather weak. This can be rationalized by considering the intersection at which the tip of the wormhole has arrived (Figure 3). One of the pores (corresponding to the wormhole path) now has a much larger flow rate than the other. In such a case, both mixing rules will give effectively the same result, providing the two outlet pores with a very similar concentration as in the leading inlet pore.

For smaller heterogeneities ($\sigma^2 = 0.002$) but the same range of relatively large Damköhler numbers, $Da_{eff} \geq 0.5$, we observe the appearance of regular, Y-shaped patterns. These patterns consist of two dominant branches growing along the lattice directions, angled at ±45° with respect to the flow. For the system with full mixing, it can be shown (Budek & Szymczak, 2012) that once such a configuration is formed, it will continue to propagate since the reactant flux in the pores parallel to the arms will always be larger than that in differently oriented pores around the channel tip. However, with streamline routing, the transition to Y-shaped patterns takes place later, at larger Da_{eff}, because streamline routing more strongly focuses reactants in the flow direction. Such focusing effect increases as the network heterogeneity decreases. This is evidenced, for example, by the pattern observed at $\sigma^2 = 0.002$ and $Da_{eff} = 0.5$, which shows straight fingers with characteristic splittings near the tips, where the side-branches angled at ±45° appear and grow for a short time, eventually dying off. At an even higher Damkohler number, $Da_{eff} = 1.0$, the two patterns (straight and angled) coexist, with small straight fingers forming first near the inlet, only to give way to Y-shaped channels, which emerge from their side-branches. This is because

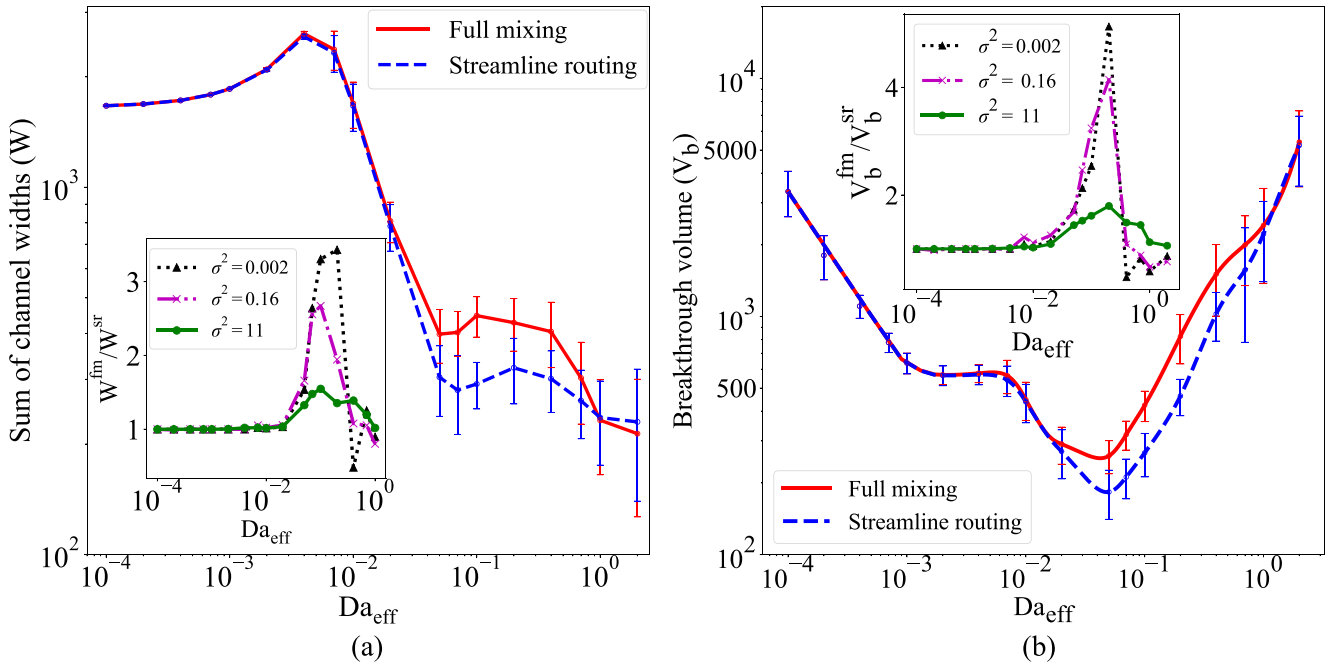

Figure 4. (a) The width of the pattern (W) versus effective Damköhler number Da_{eff} for a network of 200 × 200 nodes with the transport parameter G = 1 and heterogeneity $\sigma^2 = 11$. The simulations were run with full mixing (red line) and streamline routing (blue dashed line). The points present averages over 10 realizations of the initial disorder in the network, along with the respective error bars. In the inset, the ratio of the total pattern widths with full mixing and streamline routing, (W^{fm}/W^{sr}), is plotted versus Da_{eff} for different heterogeneities ($\sigma^2 = 0.002, 0.16, 11$). (b) Breakthrough volume (V_b) dependence on the Damköhler number for 200 × 200 network with the transport parameter G = 1 and heterogeneity $\sigma^2 = 11$ for both full mixing (red line) and streamline routing (blue dashed line). The points represent averages over 10 simulations, along with the respective error bars. In the inset, the ratio of full mixing breakthrough volume to streamline routing volume $\left(V_b^{fm}/V_b^{sr}\right)$ is shown for different heterogeneities.

a very short penetration length diminishes the mixing effect by increasing the network heterogeneity near the dissolution front.

To quantitatively characterize the channel widths in the patterns shown in Figure 2, we introduce the total width of the pattern, defined as a sum of the diameters of pores along the mid-line ($x = L_x/2$) of the network, $W = \sum_i d_i$, where d_i are the diameters of the pores intersecting the mid-line. Figure 4a shows the pattern width as a function of the effective Damköhler number for a range of different heterogeneities. As observed, both in the low and high Da_{eff} regime, W values are insensitive to the mixing protocol. However, in the intermediate regime $10^{-2} < Da_{eff} < 1$, streamline routing results in significantly thinner dissolution channels. The inset of Figure 4a shows the ratio of the widths between the two mixing protocols (W^{fm}/W^{sr}) for different initial heterogeneities (σ^2), clearly showing the mixing effect being maximized at the intermediate Da regime. These results also clearly depend on initial sample heterogeneity with a maximum effect of the mixing observed at the smallest heterogeneity.

We also investigate the effect of both mixing rules on the total volume of reactive fluid, V_b, that must be injected into the pores to obtain the breakthrough of the dissolution front. The breakthrough is defined as the moment when at least one of the outlet pores has broadened 5 times with respect to its initial diameter. Here, we use the term "breakthrough" in a chemical engineering sense, denoting the moment when the permeability of the system increases dramatically as the longest dissolution channel reaches the outlet. Note that this is different from how the term "breakthrough" is commonly used in hydrology, which denotes the moment when the tracer reaches the sampling point. The dependence of V_b on Da_{eff} is particularly important for the optimization of the dissolution of carbonate reservoirs to increase the permeability with minimum expense of reactants (Cohen et al., 2008; Fredd & Fogler, 1998; Golfier et al., 2002; Kalia & Balakotaiah, 2007; Panga et al., 2005).

Figure 4b shows $V_b(Da_{eff})$ dependence for both types of mixing rules for heterogeneity $\sigma^2 = 11$. The breakthrough volume V_b increases both for the low ($Da_{eff} < 10^{-2}$) and high ($Da_{eff} > 1$) Damköhler numbers, with similar values for both types of mixing rules. These regimes are known to be far from optimal with respect to the reactant

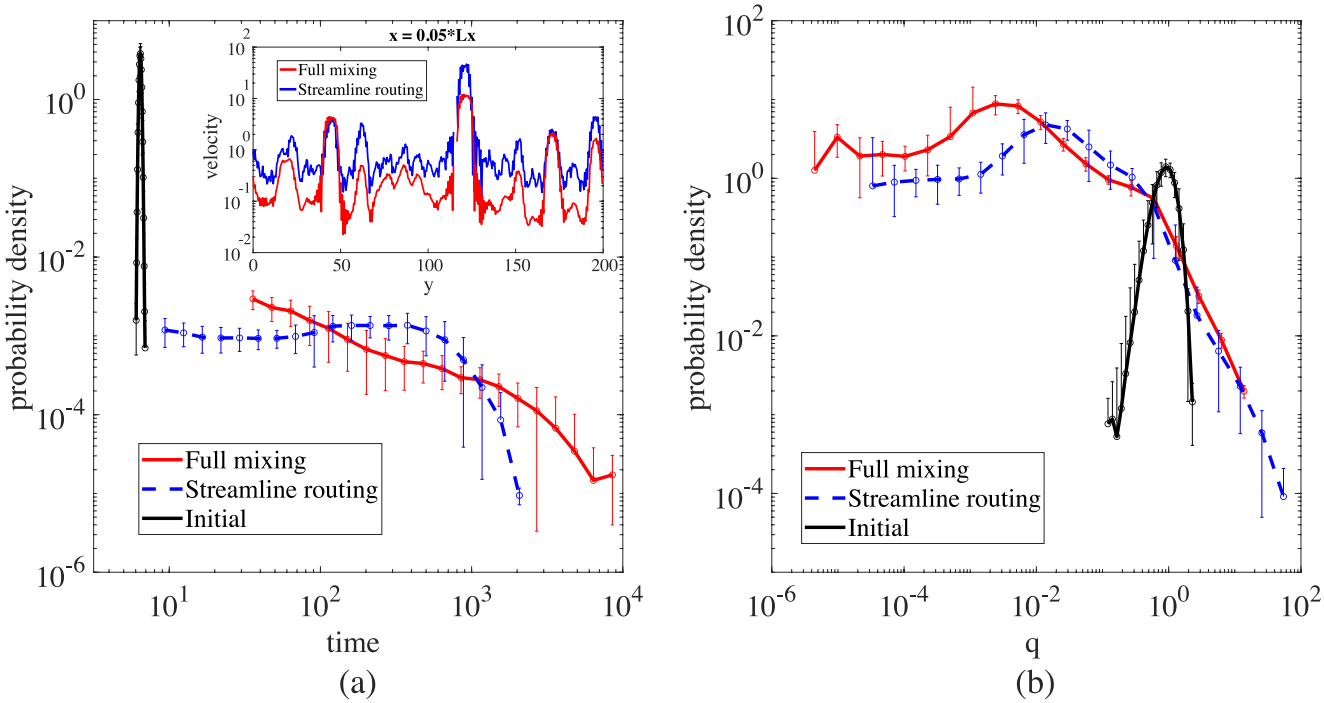

Figure 5. (a) Tracer breakthrough curves before (black line) and after dissolution at half breakthrough time at $Da_{eff} = 0.1$ and $\sigma^2 = 0.16$ for both full mixing (red line) and streamline routing (blue dashed line). The points represent averages over 10 simulations, along with the respective error bars. The inset shows the velocity magnitude along the *y*-direction (direction perpendicular to the flow direction) at $x = 0.05L_x$. (b) Probability density distributions of volumetric flux q before (black line) and after dissolution at half breakthrough time at $Da_{eff} = 0.1$ and $\sigma^2 = 0.16$ for both full mixing (red line) and streamline routing (blue dashed line). The points present averages over 10 simulations, along with the respective error bars.

volume needed to open up the system. For small Da_{eff} the dissolution is almost uniform throughout the network, hence a lot of reactant is needed to dissolve all the available pore surfaces. On the other extreme, for large Da_{eff}, the dissolution concentrates at the inlet face of the sample, which results in exceedingly long dissolution times.

However, in the moderate Da_{eff} number regime, strong competition for reactant among growing pores leads to the formation of dominant channels, which are very effective conduits for the reactant. In this regime, we found that streamline routing not only affects the shape of the channels but also minimizes the reactant volume needed for breakthrough. As shown in the inset of Figure 4b, this effect is the strongest for nearly homogeneous system ($\sigma^2 = 0.002$), where the breakthrough for the streamline routing can be as much as five times lower than that in the full mixing case. As the system heterogeneity increases, the effect of mixing protocol diminishes but even with the largest heterogeneity ($\sigma^2 = 11$) there can still be a factor of two difference between the breakthrough volumes (inset of Figure 4b).

We finally simulate passive solute (tracer) transport by particle tracking to highlight how the macroscopic dissolution patterns resulting from the two different mixing rules lead to distinctive transport behaviors. Tracer particles are advected with the mean flow velocity between nodes, and they follow either complete mixing or incomplete mixing rules at pore junctions. The details of the implementation of tracer transport can be found in Kang et al., 2015. We take flow fields at the end of each simulation, which is at the half breakthrough time, and run particle tracking simulations to obtain tracer breakthrough curves at the outlet. Figure 5a shows tracer breakthrough curves that are obtained by plotting the probability density of the individual particle arrival times at the outlet. Dissolution leads to much broader distributions compared to the initial distribution (black line), and the two mixing rules lead to distinctively different breakthrough curves (blue and red lines). Streamline routing leads to more focused flow, leading to earlier breakthroughs of tracers. On the other hand, full mixing has a stronger tailing due to slower velocity zones as shown in the inset of Figure 5a. Figure 5b shows flux distributions, further confirming the faster flow zones in the streamline routing case and the slower flow zones in the full mixing case. It is noteworthy that the breakthrough curves were distinctively different even at the highest initial heterogeneity of $\sigma^2 = 11$ (not shown).

4. Conclusions

Dissolution of porous medium by an infiltrating reactive fluid is a prime example of a process where pore scales couple to the core- or even reservoir scales. This coupling is particularly pronounced in the unstable regime, which is characterized by the emergence of dissolution channels. This work shows that the shapes and propagation velocities of these channels are sensitive to the details of the mixing process at pore intersections. When the reactant follows the streamlines, with not enough time to mix diffusively at the intersections, the flow focusing at the tips of the channels is significantly enhanced and they propagate faster, thus decreasing the breakthrough time. These effects are the strongest in the intermediate Damköhler number regime, where the reactive and advective timescales are similar. Both for larger and smaller Damköhler numbers, the effect of mixing on the dissolution patterns becomes weaker, but for different reasons. At small Da_{eff}, the concentration of reactant becomes uniform throughout the sample and the mixing rules become irrelevant. At large Da_{eff}, on the other hand, the wormhole tip focuses in itself a very large flow and reactant concentration, so the presence of other incoming pores no longer matters. This is because the increased network heterogeneity at the dissolution front, combined with the short penetration length, diminishes the mixing effect. Additionally, the coupling of mixing rules and the large-scale dissolution patterns led to distinctively different solute transport patterns as characterized by tracer breakthrough curves.

The general topic of pore-scale mixing effects on larger-scale reactive transport is of considerable interest due to its relevance not only in contaminant transport but also in karst formation (in particular mixing corrosion), acidization of carbonate reservoirs, and carbon mineralization. To the best of our knowledge, this is the first study that quantifies the potential importance of mixing extent at intersections on network-scale dissolution patterns and solute transport, which will contribute to improved predictability and uncertainty quantification in the reactive flow systems. Currently, pore-scale simulations have to be conducted to accurately estimate the mixing extent at intersections. The development of an effective (coarse-grained) mixing model that can quantify the mixing extent at intersections will require substantial follow-up studies which will be motivated by this study.

Data Availability Statement

All simulation data files are available in Sharma et al. (2023).

Acknowledgments
Rishabh P. Sharma and Piotr Szymczak acknowledge the support by University of Warsaw under Excellence Initiative—Research University (IDUB) program, Grant BOB-IDUB-622-92/2021. Jingxuan Deng and Peter K. Kang acknowledge the National Science Foundation (Grant EAR-2046015) and the donors of American Chemical Society Petroleum Research Fund for partial support of this research.

References

Ameri, A., Raoof, A., Blonk, N., & Cnudde, V. (2017). Detailed modeling of carbonate acidizing by coupling a multi-purpose pore-network simulator to the chemistry package PHREEQC-application to chelating agents. In *SPE Latin America and Caribbean petroleum engineering conference, SPE-185532-MS*.

Battiato, I., & Tartakovsky, D. (2011). Applicability regimes for macroscopic models of reactive transport in porous media. *Journal of Contaminant Hydrology*, *120*, 18–26. https://doi.org/10.1016/j.jconhyd.2010.05.005

Bejan, A. (1984). *Convection heat transfer*. Wiley.

Berkowitz, B., Naumann, C., & Smith, L. (1994). Mass transfer at fracture intersections: An evaluation of mixing models. *Water Resources Research*, *30*(6), 1765–1773. https://doi.org/10.1029/94wr00432

Blunt, M. J., Bijeljic, B., Dong, H., Gharbi, O., Iglauer, S., Mostaghimi, P., et al. (2013). Pore-scale imaging and modelling. *Advances in Water Resources*, *51*, 197–216. https://doi.org/10.1016/j.advwatres.2012.03.003

Bochet, O., Bethencourt, L., Dufresne, A., Farasin, J., Pédrot, M., Labasque, T., et al. (2020). Iron-oxidizer hotspots formed by intermittent oxic–anoxic fluid mixing in fractured rocks. *Nature Geoscience*, *13*(2), 149–155. https://doi.org/10.1038/s41561-019-0509-1

Budek, A., & Szymczak, P. (2012). Network models of dissolution of porous media. *Physical Review E - Statistical Physics, Plasmas, Fluids, and Related Interdisciplinary Topics*, *86*(5), 056318. https://doi.org/10.1103/physreve.86.056318

Carroll, S., Hao, Y., Smith, M., & Sholokhova, Y. (2013). Development of scaling parameters to describe CO_2-rock interactions within Weyburn-Midale carbonate flow units. *International Journal of Greenhouse Gas Control*, *16*, S185–S193. https://doi.org/10.1016/j.ijggc.2012.12.026

Chadam, D., Hoff, D., Merino, E., Ortoleva, P., & Sen, A. (1986). Reactive infiltration instabilities. *Journal of Applied Mathematics*, *36*(3), 207–221. https://doi.org/10.1093/imamat/36.3.207

Chaudhuri, A., Rajaram, H., & Viswanathan, H. (2013). Early-stage hypogene karstification in a mountain hydrologic system: A coupled thermohydrochemical model incorporating buoyant convection. *Water Resources Research*, *49*(9), 5880–5899. https://doi.org/10.1002/wrcr.20427

Cheung, W., & Rajaram, H. (2002). Dissolution finger growth in variable aperture fractures: Role of the tip-region flow field. *Geophysical Research Letters*, *29*(22), 32-1–32-4. https://doi.org/10.1029/2002gl015196

Cohen, C. E., Ding, D., Quintard, M., & Bazin, B. (2008). From pore scale to wellbore scale: Impact of geometry on wormhole growth in carbonate acidization. *Chemical Engineering and Science*, *63*(12), 3088–3099. https://doi.org/10.1016/j.ces.2008.03.021

Daccord, G. (1987). Chemical dissolution of a porous medium by a reactive fluid. *Physical Review Letters*, *58*(5), 479–482. https://doi.org/10.1103/physrevlett.58.479

Daccord, G., & Lenormand, R. (1987). Fractal patterns from chemical dissolution. *Nature*, *325*(6099), 41–43. https://doi.org/10.1038/325041a0

De Boever, E., Varloteaux, C., Nader, F. H., Foubert, A., Békri, S., Youssef, S., & Rosenberg, E. (2012). Quantification and prediction of the 3D pore network evolution in carbonate reservoir rocks. *Oil and Gas Science and Technology*, *67*(1), 161–178. https://doi.org/10.2516/ogst/2011170

Deng, H., Ellis, B. R., Peters, C. A., Fitts, J. P., Crandall, D., & Bromhal, G. S. (2013). Modifications of carbonate fracture hydrodynamic properties by CO2-acidified brine flow. *Energy and Fuels*, *27*(8), 4221–4231. https://doi.org/10.1021/ef302041s

Deng, H., Molins, S., Trebotich, D., Steefel, C., & DePaolo, D. (2018). Pore-scale numerical investigation of the impacts of surface roughness: Upscaling of reaction rates in rough fractures. *Geochimica et Cosmochimica Acta*, *239*, 374–389. https://doi.org/10.1016/j.gca.2018.08.005

Dentz, M., Le Borgne, T., Englert, A., & Bijeljic, B. (2011). Mixing, spreading and reaction in heterogeneous media: A brief review. *Journal of Contaminant Hydrology*, *120*, 1–17. https://doi.org/10.1016/j.jconhyd.2010.05.002

Dijk, P., & Berkowitz, B. (1998). Precipitation and dissolution of reactive solutes in fractures. *Water Resources Research*, *34*(3), 457–470. https://doi.org/10.1029/97wr03238

Dreybrodt, W. (1996). Principles of early development of karst conduits under natural and man-made conditions revealed by mathematical analysis of numerical models. *Water Resources Research*, *32*(9), 2923–2935. https://doi.org/10.1029/96wr01332

Ebadian, M. A., & Dong, Z. F. (1998). Forced convection, internal flow in ducts. In W. M. Rohsenow, J. P. Hartnett, & Y. I. Cho (Eds.), *Handbook of heat transfer*. McGraw-Hill.

Elkhoury, J., Detwiler, R., & Ameli, P. (2015). Can a fractured caprock self-heal? *Earth and Planetary Science Letters*, *417*, 99–106. https://doi.org/10.1016/j.epsl.2015.02.010

Elkhoury, J. E., Ameli, P., & Detwiler, R. L. (2013). Dissolution and deformation in fractured carbonates caused by flow of CO_2-rich brine under reservoir conditions. *International Journal of Greenhouse Gas Control*, *16*, S203–S215. https://doi.org/10.1016/j.ijggc.2013.02.023

Ellis, B. R., Peters, C. A., Fitts, J. P., Bromhal, G. S., McIntyre, D., Warzinski, R., & Rosenbaum, E. (2011). Deterioration of a fractured carbonate caprock exposed to CO_2-acidified brine flow. *Greenhouse Gases Sci. Technol.*, *1*(3), 248–260. https://doi.org/10.1002/ghg.25

Ewers, R. O. (1982). *Cavern development in the dimensions of length and breadth (Unpublished doctoral dissertation)*. McMaster University.

Fredd, C. N., & Fogler, H. S. (1998). Influence of transport and reaction on wormhole formation in porous media. *AIChE Journal*, *44*(9), 1933–1949. https://doi.org/10.1002/aic.690440902

Freire-Gormaly, M., Ellis, J. S., MacLean, H. L., & Bazylak, A. (2016). Pore structure characterization of Indiana limestone and pink dolomite from pore network reconstructions. *Oil & Gas Science and Technology–Revue d'IFP Energies nouvelles*, *71*(3), 33. https://doi.org/10.2516/ogst/2015004

Golfier, F., Zarcone, C., Bazin, B., Lenormand, R., Lasseux, D., & Quintard, M. (2002). On the ability of a Darcy-scale model to capture wormhole formation during the dissolution of a porous medium. *Journal of Fluid Mechanics*, *457*, 213–254. https://doi.org/10.1017/s0022112002007735

Groves, C. G., & Howard, A. D. (1994). Minimum hydrochemical conditions allowing limestone cave development. *Water Resources Research*, *30*(3), 607–615. https://doi.org/10.1029/93wr02945

Gupta, N., & Balakotaiah, V. (2001). Heat and mass transfer coefficients in catalytic monoliths. *Chemical Engineering and Science*, *56*(16), 4771–4786. https://doi.org/10.1016/s0009-2509(01)00134-8

Hanna, R. B., & Rajaram, H. (1998). Influence of aperture variability on dissolutional growth of fissures in karst formations. *Water Resources Research*, *34*(11), 2843–2853. https://doi.org/10.1029/98wr01528

Hao, Y., Smith, M., Sholokhova, Y., & Carroll, S. (2013). CO_2-induced dissolution of low permeability carbonates. Part II: Numerical modeling of experiments. *Advances in Water Resources*, *62*, 388–408. https://doi.org/10.1016/j.advwatres.2013.09.009

Hoefner, M. L., & Fogler, H. S. (1988). Pore evolution and channel formation during flow and reaction in porous media. *AIChE Journal*, *34*(1), 45–54. https://doi.org/10.1002/aic.690340107

Hu, R., Wang, T., Yang, Z., Xiao, Y., Chen, Y.-F., & Zhou, C.-B. (2021). Dissolution hotspots in fractures. *Geophysical Research Letters*, *48*(20), e2021GL094118. https://doi.org/10.1029/2021gl094118

Hull, L. C., & Koslow, K. N. (1986). Streamline routing through fracture junctions. *Water Resources Research*, *22*(12), 1731–1734. https://doi.org/10.1029/wr022i012p01731

Jamtveit, B., & Hammer, O. (2012). Sculpting of rocks by reactive fluids. *Geochemical Perspectives Letters*, *1*(3), 341–481. https://doi.org/10.7185/geochempersp.1.3

Kalia, N., & Balakotaiah, V. (2007). Modeling and analysis of wormhole formation in reactive dissolution of carbonate rocks. *Chemical Engineering and Science*, *62*(4), 919–928. https://doi.org/10.1016/j.ces.2006.10.021

Kang, P. K., Bresciani, E., An, S., & Lee, S. (2019). Potential impact of pore-scale incomplete mixing on biodegradation in aquifers: From batch experiment to field-scale modeling. *Advances in Water Resources*, *123*, 1–11. https://doi.org/10.1016/j.advwatres.2018.10.026

Kang, P. K., Dentz, M., Borgne, T. L., & Juanes, R. (2015). Anomalous transport on regular fracture networks: Impact of conductivity heterogeneity and mixing at fracture intersections. *Physical Review E - Statistical Physics, Plasmas, Fluids, and Related Interdisciplinary Topics*, *92*(2), 022148. https://doi.org/10.1103/physreve.92.022148

Kang, P. K., Dentz, M., Borgne, T. L., Lee, S., & Juanes, R. (2017). Anomalous transport in disordered fracture networks: Spatial Markov model for dispersion with variable injection modes. *Advances in Water Resources*, *106*, 80–94. https://doi.org/10.1016/j.advwatres.2017.03.024

Kang, P. K., Dentz, M., & Juanes, R. (2011). Predictability of anomalous transport on lattice networks with quenched disorder. *Physical Review E - Statistical Physics, Plasmas, Fluids, and Related Interdisciplinary Topics*, *83*(3), 030101. https://doi.org/10.1103/physreve.83.030101

Ladd, A. J., & Szymczak, P. (2021). Reactive flows in porous media: Challenges in theoretical and numerical methods. *Annual Review of Chemical and Biomolecular Engineering*, *12*(1), 543–571. https://doi.org/10.1146/annurev-chembioeng-092920-102703

Lake, L., Bryant, S., & Araque-Martinez, A. (2002). *Geochemistry and fluid flow*. Elsevier.

Lee, S. H., & Kang, P. K. (2020). Three-dimensional vortex-induced reaction hot spots at flow intersections. *Physical Review Letters*, *124*(14), 144501. https://doi.org/10.1103/physrevlett.124.144501

Lee, W., Yoon, S., & Kang, P. K. (2023). Inertia and diffusion effects on reactive transport with fluid-solid reactions in rough fracture flows. *Physical Review Fluids*, *8*(5), 054502. https://doi.org/10.1103/physrevfluids.8.054502

Li, L., Peters, C. A., & Celia, M. A. (2006). Upscaling geochemical reaction rates using pore-scale network modeling. *Advances in Water Resources*, *29*(9), 1351–1370. https://doi.org/10.1016/j.advwatres.2005.10.011

Li, L., Peters, C. A., & Celia, M. A. (2007). Effects of mineral spatial distribution on reaction rates in porous media. *Water Resources Research*, *43*(1), W01419. https://doi.org/10.1029/2005wr004848

Liu, M., Kwon, B., & Kang, P. K. (2022). Machine learning to predict effective reaction rates in 3D porous media from pore structural features. *Scientific Reports*, *12*(1), 5486. https://doi.org/10.1038/s41598-022-09495-0

Luquot, L., & Gouze, P. (2009). Experimental determination of porosity and permeability changes induced by injection of CO_2 into carbonate rocks. *Chemical Geology*, *265*(1–2), 148–159. https://doi.org/10.1016/j.chemgeo.2009.03.028

Luquot, L., Rodriguez, O., & Gouze, P. (2014). Experimental characterization of porosity structure and transport property changes in limestone undergoing different dissolution regimes. *Transport in Porous Media*, *101*(3), 507–532. https://doi.org/10.1007/s11242-013-0257-4

Maheshwari, P., & Balakotaiah, V. (2013). Comparison of carbonate HCI acidizing experiments with 3D simulations. *SPE Production & Operations*, *28*(04), 402–413. https://doi.org/10.2118/164517-pa

Menke, H., Andrew, M., Blunt, M., & Bijeljic, B. (2016). Reservoir condition imaging of reactive transport in heterogeneous carbonates using fast synchrotron tomography—Effect of initial pore structure and flow conditions. *Chemical Geology*, *428*, 15–26. https://doi.org/10.1016/j.chemgeo.2016.02.030

Menke, H., Bijeljic, B., & Blunt, M. (2017). Dynamic reservoir-condition microtomography of reactive transport in complex carbonates: Effect of initial pore structure and initial brine ph. *Geochimica et Cosmochimica Acta*, *204*, 267–285. https://doi.org/10.1016/j.gca.2017.01.053

Motyka, I., & Wilk, Z. (1984). Hydraulic structure of karst-fissured Triassic rocks in the vicinity of Olkusz (Poland). *Kras i Speleologia*, *14*, 11–24.

Nogues, J. P., Fitts, J. P., Celia, M. A., & Peters, C. A. (2013). Permeability evolution due to dissolution and precipitation of carbonates using reactive transport modeling in pore networks. *Water Resources Research*, *49*(9), 6006–6021. https://doi.org/10.1002/wrcr.20486

Noiriel, C., Gouze, P., & Made, B. (2013). 3D analysis of geometry and flow changes in a limestone fracture during dissolution. *Journal of Hydrology*, *486*, 211–223. https://doi.org/10.1016/j.jhydrol.2013.01.035

Paillet, F. L., Hess, A. E., Cheng, C. H., & Harding, E. (1987). Characterization of fracture permeability with high-resolution vertical flow measurements during borehole pumping. *Ground Water*, *25*(1), 28–40. https://doi.org/10.1111/j.1745-6584.1987.tb02113.x

Palmer, A. N. (1991). Origin and morphology of limestone caves. *The Geological Society of America Bulletin*, *103*(1), 1–21. https://doi.org/10.1130/0016-7606(1991)103<0001:oamolc>2.3.co;2

Panga, M. K. R., Ziauddin, M., & Balakotaiah, V. (2005). Two-scale continuum model for simulation of wormholes in carbonate acidization. *AIChE Journal*, *51*(12), 3231–3248. https://doi.org/10.1002/aic.10574

Park, Y.-J., Lee, K.-K., & Berkowitz, B. (2001). Effects of junction transfer characteristics on transport in fracture networks. *Water Resources Research*, *37*(4), 909–923. https://doi.org/10.1029/2000wr900365

Polak, A., Elsworth, D., Liu, J., & Grader, A. S. (2004). Spontaneous switching of permeability changes in a limestone fracture with net dissolution. *Water Resources Research*, *40*(3), W03502. https://doi.org/10.1029/2003wr002717

Raoof, A., Nick, H., Wolterbeek, T., & Spiers, C. (2012). Pore-scale modeling of reactive transport in wellbore cement under CO2 storage conditions. *International Journal of Greenhouse Gas Control*, *11*, S67–S77. https://doi.org/10.1016/j.ijggc.2012.09.012

Roded, R., Aharonov, E., Holtzman, R., & Szymczak, P. (2020). Reactive flow and homogenization in anisotropic media. *Water Resources Research*, *56*(12), e2020WR027518. https://doi.org/10.1029/2020wr027518

Roded, R., Szymczak, P., & Holtzman, R. (2021). Wormholing in anisotropic media: Pore-scale effect on large-scale patterns. *Geophysical Research Letters*, *48*(11), e2021GL093659. https://doi.org/10.1029/2021gl093659

Rowan, G. (1959). Theory of acid treatment of limestone formations. *Journal of the Institute of Petroleum*, *45*(431), 321.

Saffman, P. G. (1959). A theory of dispersion in a porous medium. *Journal of Fluid Mechanics*, *6*(03), 321. https://doi.org/10.1017/s0022112059000672

Sanchez-Vila, X., Guadagnini, A., & Carrera, J. (2006). Representative hydraulic conductivities in saturated groundwater flow. *Reviews of Geophysics*, *44*(3), RG3002. https://doi.org/10.1029/2005rg000169

Sharma, R. P., Kang, P. K., & Szymczak, P. (2023). Effects of mixing at pore intersections on large-scale dissolution patterns [Dataset]. Zenodo. https://doi.org/10.5281/zenodo.7677027

Sherman, T., Hyman, J. D., Bolster, D., Makedonska, N., & Srinivasan, G. (2019). Characterizing the impact of particle behavior at fracture intersections in three-dimensional discrete fracture networks. *Physical Review E - Statistical Physics, Plasmas, Fluids, and Related Interdisciplinary Topics*, *99*(1), 013110. https://doi.org/10.1103/physreve.99.013110

Steefel, C. I., & Lasaga, A. C. (1990). Evolution of dissolution patterns. In D. C. Melchior & R. L. Bassett (Eds.), *Chemical modeling of aqueous systems II* (pp. 212–225). Am. Chem. Soc.

Steefel, C. I., & Maher, K. (2009). Fluid-rock interaction: A reactive transport approach. *Reviews in Mineralogy and Geochemistry*, *70*(1), 485–532. https://doi.org/10.2138/rmg.2009.70.11

Stockman, H. W., Johnson, J., & Brown, S. R. (2001). Mixing at fracture intersections: Influence of channel geometry and the Reynolds and Peclet numbers. *Geophysical Research Letters*, *28*(22), 4299–4302. https://doi.org/10.1029/2001gl013287

Szymczak, P., & Ladd, A. J. C. (2009). Wormhole formation in dissolving fractures. *Journal of Geophysical Research*, *114*(B6), B06203. https://doi.org/10.1029/2008jb006122

Szymczak, P., & Ladd, A. J. C. (2011). The initial stages of cave formation: Beyond the one-dimensional paradigm. *Earth and Planetary Science Letters*, *301*(3–4), 424–432. https://doi.org/10.1016/j.epsl.2010.10.026

Tansey, J., & Balhoff, M. T. (2016). Pore network modeling of reactive transport and dissolution in porous media. *Transport in Porous Media*, *113*(2), 303–327. https://doi.org/10.1007/s11242-016-0695-x

Upadhyay, V. K., Szymczak, P., & Ladd, A. J. C. (2015). Initial conditions or emergence: What determines dissolution patterns in rough fractures? *Journal of Geophysical Research: Solid Earth*, *120*(9), 6102–6121. https://doi.org/10.1002/2015jb012233

Worthington, S. R. H., & Ford, D. C. (2009). Self-organized permeability in carbonate aquifers. *Ground Water*, *47*(3), 326–336. https://doi.org/10.1111/j.1745-6584.2009.00551.x

Xiong, Q., Baychev, T. G., & Jivkov, A. P. (2016). Review of pore network modelling of porous media: Experimental characterisations, network constructions and applications to reactive transport. *Journal of Contaminant Hydrology*, *192*, 101–117. https://doi.org/10.1016/j.jconhyd.2016.07.002

Zou, L., Jing, L., & Cvetkovic, V. (2017). Modeling of flow and mixing in 3D rough-walled rock fracture intersections. *Advances in Water Resources*, *107*, 1–9. https://doi.org/10.1016/j.advwatres.2017.06.003